Geophys. J. Int. (1992) **109,** 376–390

Revised hypocentre and fault rupture geometry for the 1980 November 23 Campania–Basilicata earthquake in southern Italy

Rob Westaway
Department of Geological Sciences, University of Durham, South Road, Durham DH1 3LE, *UK*

Accepted 1991 November 13. Received 1991 May 29; in original form 1991 January 30

SUMMARY

The fault rupture nucleation point of the 1980 November 23 Campania–Basilicata earthquake is relocated, following the recent identification of ~20 km of surface faulting, the Carpineta and Picentini fault scarps, in addition to the ~15 km previously documented on the Marzano and San Gregorio faults, all of which have ~NW strike and ~60° NE dip. This relocation indicates a range of revised origin times and nucleation point positions at 10–12 km depth that are ~5–9 km SE of previously documented coordinates, between 18:34:52.0 ± 0.3 s, with latitude 40.724° ± 1.4 km and longitude 15.414° ± 1.4 km (preferred), and 18:34:52.5 ± 0.3 s, with latitude 40.742° ± 1.4 km and longitude 15.373° ± 1.4 km. My preferred nucleation point coincides with a downdip projection of the SE end of the Carpineta fault and indicates that this fault ruptured first, rather than the Marzano fault as was previously thought.

With the fault rupture nucleation point adjusted to this new preferred position, field and seismological estimates of seismic moment match well, both overall and for individual fault scarps, and suggest the following sequence of fault rupture subevents. The initial fault rupture nucleated at or near the SE end of the Carpineta fault and propagated NW, releasing $\sim 2.5 \times 10^{18}$ N m seismic moment. Rupture continued apparently without interruption onto the adjoining Marzano fault farther NW, where $\sim 6.5 \times 10^{18}$ N m of seismic moment was released. Rupture then paused for ~0.5 s, before continuing NW along the Picentini fault, where $\sim 4.5 \times 10^{18}$ N m more seismic moment was released. Probably early in this sequence of NW-propagating ruptures, a SE-propagating rupture released $\sim 2 \times 10^{18}$ N m seismic moment on the San Gregorio fault. Each of these fault scarps and the corresponding rupture subevent was associated with intense aftershock activity. The existence of another aftershock cluster NW of the Picentini scarp suggests a fifth mainshock rupture subevent, at Castelfranci, which released up to $\sim 2 \times 10^{18}$ N m more seismic moment. Rupture at this locality appears necessary to explain the form of ground acceleration recorded nearby, also.

Following these ruptures on steep NE-dipping normal faults, two additional ruptures occurred on faults with different orientations, ~20 s and ~40 s after the initial mainshock rupture. The 40 s subevent involved release of $\sim 3 \times 10^{18}$ N m of seismic moment on a steep normal fault that dips SW at ~70° and projects to the earth's surface ~11 km NE of the Marzano fault. The 20 s subevent apparently involved release of $\sim 4 \times 10^{18}$ N m of seismic moment on a surface dipping NE at ~20°, at the base of the brittle upper crust beneath this steep antithetic fault.

Points where normal fault ruptures nucleated on the steep NE-dipping normal faults coincide with *en echelon* steps of >~1 km and abrupt ~15° changes in strike. The Marzano and Carpineta faults, which have strike ~315°, took up a small component of left-lateral slip, as is revealed by the first-motion focal mechanism, teleseismic waveform modelling, striations measured in the field, and consistent

rightward stepping: their slip vector azimuth is ~N37°E. Assuming the same slip vector azimuth, a component of right-lateral slip is expected on the San Gregorio and Picentini faults that have strike ~300°.

Key words: Apennines, Campania, continental extension, earthquake, Italy, normal faulting.

1 INTRODUCTION

The Campania–Basilicata earthquake at 18:52 on 1980 November 23 was the largest (M_s 6.9; M_o 26×10^{18} N m) normal-faulting event in the Apennine mountains of Italy for over 60 yr. Because normal-faulting earthquakes of this size are relatively rare, studies of this event contribute not only to knowledge of the active tectonics of Italy, but also to the understanding of continental extension in general.

Westaway & Jackson (1987) published a set of results concerning this earthquake that documented information then available. These included, first, a description of ~15 km of surface faulting, the Marzano and San Gregorio fault scarps, with ~60° NE dip and ~NW strike, which had earlier been reported by Westaway & Jackson (1984). Second, we (1987) attempted forward modelling of long-period teleseismic waveforms, with the aim of correlating seismogram complexity with observed complexity of surface faulting and other structure in the epicentral region. This waveform modelling established that additional faulting probably occurred that had not then been identified at the earth's surface. Third, we examined records of ground acceleration from the epicentral region, attempting to use the timing of seismic pulses in these accelerograms to constrain the relative positions of two later fault rupture subevents (which occurred ~20 s and ~40 s after rupture initiated) more tightly than was possible from teleseismic observations. We suggested that these two late subevents involved rupture on very low-angle surfaces at the base of the upper crustal brittle layer, with dip ~20° to the NE. We also considered the 1980 aftershock sequence in detail, showing that it persisted northwestward way beyond the documented surface faulting. This aftershock activity included a relatively dense cluster more than ~20 km NW of the documented surface faulting (Westaway & Jackson 1987, fig. 23a) near Castelfranci, which had more northerly trend (~330°) than the rest of the aftershock zone. No aftershock had magnitude >~5, and the cumulative deformation associated with aftershocks was negligible. Any observed surface faulting was thus almost certainly produced by the mainshock. Finally, we discussed observations of elevation change that were obtained by relevelling following the earthquake and were first documented by Arca *et al.* (1983). Westaway (1987b) had already shown that part of this data set was unreliable, with elevation change caused by landsliding and not by tectonic deformation.

Subsequent studies have increased understanding of some aspects of this earthquake far beyond what we (1987) achieved. Pantosti & Valensise (1990a) reported ~20 km of additional surface faulting, much of which was along the front of the Picentini range (Westaway & Jackson 1987, plate 1) where we (1984, 1987) had predicted it. Pantosti & Valensise (1990b) presented results of trenching across the Marzano scarp that establish ~1700 yr recurrence interval for earthquakes similar to the 1980 event. This recurrence history is shared by the San Gregorio fault, and presumably also by the intervening Carpineta fault. Documented local historical earthquakes that were comparable to the 1980 event, such as those on 1694 September 8 (see, e.g., Westaway & Jackson 1987, fig. 26; Postpischl 1985) and in AD 990 (Postpischl 1985), thus did not rupture these faults.

Bernard & Zollo (1989) proposed a different scheme for the relative timings and relative positions of the initial rupture and the 20 and 40 s subevents. Their position for the 40 s subevent was not far from ours—~10 km NE of the Marzano fault scarp—but they suggested instead that this subevent occurred on a steep antithetic normal fault dipping SW. A source with this orientation has a similar far-field (teleseismic) radiation pattern to that which we (1987) proposed for this subevent. However, near-field seismological studies by Bernard & Zollo (1989), which could resolve this nodal plane ambiguity, established that the relatively steep plane dipping SW was the fault plane. Pantosti & Valensise (1990a) reached a similar conclusion, which I now accept, following elastic dislocation modelling of the portion of the elevation change data set from near this locality, which they considered reliable.

The same degree of certainty cannot be said to have been reached by investigations of the 20 s subevent. Bernard & Zollo's (1989) study of its timing proposed a radically different position from ours: ~20 km SE of our (1987) fault rupture nucleation point. They suggested that this 20 s subevent involved rupture of the southeasternmost observed surface faulting near San Gregorio. However, because this faulting had ~60° NE dip at the earth's surface (Westaway & Jackson 1984, 1987), they were obliged to conclude that this fault flattened to 20° dip at shallow depth to explain our (1987) teleseismic waveform modelling. They suggested that this lower dip is supported by elastic dislocation modelling of elevation changes near their suggested position of this fault plane. However, recalling the problems that exist elsewhere with this elevation change data set (Westaway 1987b; Pantosti & Valensise 1990a), it appears unwise to have faith in it without supporting evidence, particularly since no-one appears to have scrutinized the reliability of the part of it near San Gregorio. Furthermore, it is difficult to explain why the San Gregorio fault should be strongly listric when others along strike from it are planar, with ~60° dip, to the base of the brittle upper crust (Westaway & Jackson 1987; Pantosti & Valensise 1990a). Finally, aftershock activity was negligible near much of Bernard & Zollo's (1989) suggested 20° dipping fault plane, indicating that a major fault with this position and orientation is most unlikely to have ruptured in the mainshock. In contrast, the compact width in the NE direction of the aftershock cluster near San Gregorio (Westaway & Jackson 1987) indicates

strongly that the fault that ruptured there was very steep throughout the brittle layer.

Although they noted some of these problems, Pantosti & Valensise (1990a) nonetheless accepted that the 20 s subevent satisfied the timing scheme suggested by Bernard & Zollo (1989) and therefore probably was associated with the San Gregorio scarp. Their view (which I support) that this fault is steep, if combined with this suggested position (which I do not support), requires the conclusion that our (1987) teleseismic waveform modelling is incapable of distinguishing 20° from 60° NE dip. However, assuming shear modulus 3×10^{10} Pa, the 4×10^{18} N m seismic moment observed teleseismically in the 20 s subevent (Westaway & Jackson 1987) would require ~2 m average coseismic slip, given the <~7 km length of the San Gregorio scarp (Pantosti & Valensise 1990a), its 60° dip, and its ~10 km vertical extent. Elastic dislocation modelling of coseismic deformation (e.g., Ward & Barrientos 1986; Pantosti & Valensise 1990a) suggests that, for a 60° dipping normal fault, slip at the earth's surface is roughly half that at depth. The 1 m high scarp at the earth's surface on the Marzano fault indeed appears to have been caused by ~2 m *maximum* slip at depth (Pantosti & Valensise 1990a). However, it is difficult to reconcile the ~0.5 m high scarp observed at the earth's surface at San Gregorio with 2 m *average* slip at depth, which would be required if 4×10^{18} N m seismic moment was released on the San Gregorio fault. In addition, the teleseismic radiation from the 20 s subevent shows strong azimuthal variations in amplitude, and requires unusually long source duration (>~8 s), both of which appear diagnostic of low-angle rupture at the base of the brittle layer (Eyidoğan & Jackson 1985). Furthermore, the relatively low ground acceleration for the 20 s subevent in relation to its seismic moment (Westaway & Jackson 1987) suggests that it may have involved unusual source physics, perhaps associated with relatively slow downward propagation of a rupture into the usually plastic uppermost lower crust. The 40 s subevent, in contrast, showed shorter source duration (~4 s), and was always the weaker candidate for a very low-angle rupture.

Panza & Suhadolc (1989) also suggested that a rupture occurred near the San Gregorio scarp ~20 s after the first rupture initiated. Inclusion of this rupture had a dramatic effect on their synthetic accelerograms at stations Auletta and Brienza, southeast of the surface faulting. However, these synthetic accelerograms bear little resemblence to those observed at these stations. Furthermore, their (1989) timing scheme for the set of accelerograms differs substantially from that by Bernard & Zollo (1989) and by Westaway & Jackson (1987). Thus, although both Panza & Suhadolc (1989) and Bernard & Zollo (1989) support the San Gregorio fault having slipped ~20 s after the initial rupture, their reasons are mutually inconsistent. No convincing evidence links the 20 s subevent observed teleseismically with the San Gregorio scarp.

Ideas concerning the 20 s subevent have recently been complicated further by Harabaglia, Suhadolc & Panza (1990), who proposed yet another timing scheme for the accelerograms, which differs considerably from those by Westaway & Jackson (1987), Panza & Suhadolc (1989), and Bernard & Zollo (1989). Given that these records do not have absolute timing, it is unlikely to ever be possible to uniquely resolve their timing, and it therefore probably makes sense for future ground acceleration investigations to treat this timing as a free parameter to be optimized within source models, rather than assuming one of the schemes already proposed.

Despite this controversy concerning some source parameters for the Campania–Basilicata earthquake, some of our other (1987) parameters have apparently been accepted without question. One of the most important is our preferred position for the fault rupture nucleation point (location 4 in Table 1), which was obtained relative to one of the larger aftershocks that was located to high precision using data from a dense temporary network of portable seismographs that was deployed after the main shock. The main purpose of this article, as described in Section 2, is to demonstrate that a revised location method along with more careful scrutiny of the available *P*-wave arrival time data gives a significantly different nucleation point. The implications of this result for understanding this earthquake are discussed in Section 3.

2 NUCLEATION POINT OF THE INITIAL FAULT RUPTURE

Review of previous locations

I am unaware of any study that has attempted independently to locate the fault rupture nucleation point of the Campania–Basilicata earthquake since Westaway & Jackson (1987), or even of any that has checked our (1987) results. These were based on a relative location procedure by Westaway (1987a) that assumes that both the master and secondary events occurred at the same focal depth (or alternatively, that any difference in their focal depths is small compared with their horizontal separation). We (1987) suggested that the initial fault rupture in the 1980 mainshock nucleated probably at ~12 km depth, at the base of the brittle layer, and had centroid depth ~10 km, indicating a component of upward rupture propagation. Locations of the mainshock nucleation point and the aftershock used as a master event, including those from agency bulletins and from our (1987) results, are listed in Table 1.

Routine agency locations for both the mainshock and this aftershock are ~10 km north of the locations suggested by local studies. This systematic error is caused by the uneven station distribution, and is a well-established problem for many agency locations of Mediterranean earthquakes (see e.g. Westaway & Jackson 1987): most permanent seismograph stations are situated to the north or northwest on the focal sphere (see, e.g., fig. 3 of Westaway & Jackson 1987). Origin time, focal depth, and latitude trade off strongly between the different locations, and careful thought thus needs to be given to determining preferred values for these parameters. The low formal standard errors for our (1987) aftershock epicentre, ~0.8 km, reflect the large number of seismographs in the temporary network (37), most of which (27) recorded this event, the use of some (7) *S*-wave arrival time data, and the use of station corrections to partially account for lateral variations in structure beneath different stations. This aftershock location is potentially questionable given that it was not obtained using a proper 3-D velocity model. However, the principal lateral

Table 1. Locations of the mainshock nucleation point and the aftershock used as master.

Time	Latitude	Longitude	Depth	N	Ref
	Mainshock nucleation point; 1980 November 23				
18:34:53.8	40.9	15.4	10 (fixed)	265	NEIS
18:34:52.2 • 0.1	40.86 • 1.4	15.33 • 1.1	0 (fixed)	506	ISC
18:34:52.8 • 0.3	40.762 • 2.4	15.332 • 2.5	15.2 • 2.6	32	WJ87 (3)
• 0.1	40.778 • 1.7	15.332 • 1.6	(12) (fixed)	63	WJ87 (4)
18:34:52.0 • 0.3	40.724 • 1.4	15.414 • 1.4	12 • 2	46	This study A
18:34:52.5 • 0.3	40.742 • 1.4	15.373 • 1.4	12 • 2	46	This study B
	Aftershock; 1980 December 8 (m_b 4.6)				
02:49:39.6	40.9	15.3	10 (fixed)		NEIS
02:49:40.1 • 0.34	40.88 • 3.5	15.29 • 3.4	10 (fixed)	81	ISC
02:49:40.0 • 0.1	40.805* • 0.8	15.229* • 0.8	12 • 2	27	WJ87
02:49:40.0 • 0.3	40.805* • 0.8	15.229* • 0.8	12 • 2	27	This study

NEIS, ISC, and WJ87 denote bulletins of the US National Earthquake Information Service and the International Seismological Centre, and Westaway & Jackson (1987). Note that the aftershock origin time was listed incorrectly by WJ87: the correct time, from appendix G of Westaway (1985), is quoted here. The aftershock location from this study is derived from that by WJ87; uncertainty in latitude and longitude δx_i $(i = 1,2)$ are retained as before, though the estimated uncertainty in origin time is increased following discussion in the text. Mainshock locations A and B are derived from the relative locations obtained by fitting curves A and B to the data in Fig. 2(b), taking account of the preferred aftershock location. For each of these, listed nominal uncertainty in origin time δT_o is the same as for the aftershock, and uncertainty in position is calculated, assuming errors in aftershock position and origin time are uncorrelated, as the square root of $(2\delta T_o/v_m)^2 + \delta x_i^2$.

variation in velocity structure in the epicentral area is the relative slowness of velocity northeast of the 1980 surface faulting, compared with other azimuths, which if not corrected for will cause aftershock locations to be too far southwest (Bernard & Zollo 1989). This may offset the resulting relative location of the mainshock southwest of its true position. However, the main issue that I am pursuing here is the uncertainty in location of the 1980 mainshock relative to this aftershock. Because of the independence of the methods used, this is independent of uncertainty in the aftershock location. Furthermore, the principal contention, which concerns the separation of the mainshock and aftershock in the southeastward direction, is independent of any northeastward mislocation of the aftershock caused by any failure to account for the principal lateral variation in velocity structure in the epicentral area.

The International Seismological Centre (ISC) aftershock location is ~10 km NNE of our (1987) location, and has origin time 1.3 s later (Table 1). Our (1987) aftershock location was obtained using a velocity model in which velocity increased linearly with depth. The typical ray geometry for this structure (see fig. 3.2.4 of Westaway 1985) means that rays leaving a source at 10 km depth to stations with ~34 km epicentral distance will take off upward. Given the ~60 km diameter of the temporary seismograph network (see fig. 3.1.1 of Westaway 1985), and given that the epicentre of the aftershock used as a master event was near the centre of this network, rays to most stations that recorded this aftershock took off upwards. This means that if its depth were adjusted shallower from 12 to say 10 km, the origin time obtained using this temporary network would adjust slightly later. The later ISC origin time is explained by the higher latitude of their epicentre relative to ours, which is nearer most permanent seismograph stations that recorded the aftershock. Overall, taking all these observations into account, the depth of this aftershock can be conservatively assessed as ~10–12 km, and its origin time appears to have been within ~0.3 s of 02:49:40 on 1980 December 8.

Using the relative location method of Westaway (1987a), we (1987) established a preferred position for 1980 mainshock nucleation point at location 4 in Table 1, which is ~9 km toward azimuth S71°E from our location for the aftershock. This relative location used *P*-wave arrival times form 63 regional and teleseismic stations that reported both events. We (1987) independently located the mainshock nucleation point directly using *P*-wave arrival times at 32 regional stations, determining location 3 in Table 1, which is within 2 km of location 4 (their formal standard error ellipses overlap — see fig. 3 of Westaway & Jackson 1987). However, this direct location method is less reliable, partly because of the uneven station distribution (the shape of Italy causes most regional stations to be either to the NW—the majority—or the SE) and partly because, unlike the relative location method, it assumes no lateral variations in seismic velocity. Given the station distribution, displacing this mainshock nucleation point location SE would adjust the estimated mainshock origin time slightly earlier, closer to the times that we deduce in this study (Table 1).

The US National Earthquake Information Service (NEIS) epicentre for the mainshock is ~15 km north of our (1987) preferred epicentre. As for the ISC and NEIS aftershock locations, its relatively late origin time is explicable as a result of systematic northward mislocation. The ISC mainshock location is not only too far north (which, on its own, would make the origin time late) but also is fixed at the earth's surface, rather than at the more realistic ~10 km depth (which, on its own, given the downward propagation of *P*-wave ray paths from it, would make the origin time early). These two sources of systematic error in origin time for this ISC location appear to largely cancel, giving an origin time that is a few tenths of a second earlier than that for our (1987) location using regional stations (location 3 in Table 1).

Revised location method

As was shown quantitatively by Westaway (1987a), if one assumes that two earthquakes have the same focal depth then their relative *P*-wave arrival time will vary sinusoidally with ray path azimuth, and is proportional to their separation. For a given separation and ray path azimuth, relative arrival time also varies in proportion to the sine of take-off angle relative to the downward vertical. Fig. 1 shows a typical variation of take-off angle relative to the downward vertical. Fig. 1 shows a typical variation of take-off angle against epicentral distance for a crustal earthquake.

This angle remains almost constant, in this case at 58°–59°, out to distance ~800 km or ~7°, because the first *P*-wave arrival in this distance range, the *Pn* phase, is refracted along the Moho. Moving to slightly greater distances, take-off angle decreases somewhat more rapidly,

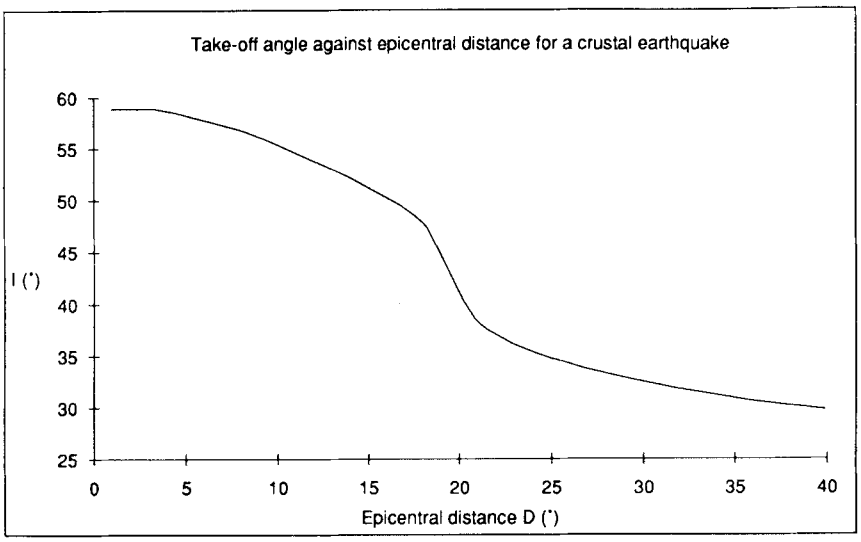

Figure 1. Graph of take-off angle against epicentral distance, calculated using Herrin (1968) *P*-wave traveltime tables for an earthquake source at 10 km depth in 33 km thick crust in which the *P*-wave velocity is 6.8 km s^{-1}. See text for discussion.

from ~58° to ~54° over ~7° to 12° distance, as ray paths start to dive gently into the upper mantle. Rays travelling to greater distances will dive progressively more steeply, with the rapid variation in take-off angle around 20° distance associated with rays that bottom out deeper in the upper mantle where *P*-wave velocity increases sharply with depth.

The method proposed here uses relative arrival time at close stations to which the upper mantle part of the ray path is subhorizontal. For these stations and for a pair of earthquakes with horizontal separation, x, peak-to-peak amplitude Δt_a of the expected sinusoidal variation of relative arrival time against ray path azimuth can readily be shown to equal $2x/v_m$, where v_m, ~8 km s^{-1}, is the *Pn*-wave velocity in the uppermost mantle.

Table 2 lists reported *P*-wave arrival times and other data from seismograph stations within 12° epicentral distance that recorded both the mainshock and the December 8 aftershock. The next nearest station that recorded both events was 19° distant, and only 10 common stations were identified between 19° and 40° distance. The 12° cut-off in distance was thus not only appropriate given Fig. 1, but is also a natural break in the available data. As noted above, the take-off angle to a station at 12° distance will be ~54°, not 59° for the *Pn* phase. However, because the ratio of sin (59°)/sin (54°) is only ~1.06, treating all data as though they had the same take-off angle will introduce only a ~6 per cent systematic error in separation predicted from the relative arrival times at the most distant stations. For this pair of earthquakes this systematic error is unimportant, because random errors in arrival times at many stations appear to be ~1 s. With Δt_a later shown to be ~4 s, some individual relative arrival time data thus have ~25 per cent random errors, which are larger than the 6 per cent maximum systematic error. If pairs of much more widely spaced earthquakes were located relative to each other instead, percentage random error in arrival times would typically be smaller, and a correction may be required for timing differences associated with different take-off angles for stations ~7°–12° distant.

Lateral variations in relative *P*-wave arrival time are evident in Table 2, and confirm the expected non-zero horizontal separation of the two events. However, relative arrival times are also potentially affected by *P*-wave picking errors and seismograph timing errors. In the absence of access to the original seismograms, one should consider objectively how to deal with these errors. A few stations show very large differences in relative arrival time compared with other stations at similar azimuths. These differences may well be caused by errors in seismograph timing. Many stations display timing using minute-marker pulses, supplemented by other pulses at 10 s intervals. These pulses may potentially be confused when seismograms are read by station operators, causing 10 and 60 s timing errors. At some more distant stations relative arrival time is smaller than expected, which is probably caused by arrival time for the aftershock being picked late. At other stations *P*-wave residuals are large, but similar, for both events.

Results

Many *P*-wave arrival times for the 1980 mainshock and aftershock fall into one or other of five categories, as indicated in Table 1. Category (1), comprising stations DUI, AQU, MNS, SDS, VAY, KHC, WET, PRU and PRA, shows non-zero residuals that are similar for the mainshock and aftershock, which may be caused by anomalous velocity structure along the ray path to the station. These differences between observed and expected traveltimes will largely cancel during relative location, and these data are therefore likely to be reliable. In Category (2), at stations PRG, VLO, ORO and SOP, the large positive residual for the aftershock suggests that its arrival time was picked late, perhaps because the amplitude of this *P*-wave was so small that its first part was missed. These data are therefore most likely unreliable, and are excluded. The focal mechanism for the aftershock, from appendix J of Westaway (1985), although not tightly constrained, was similar to that of the mainshock with a steep northeast-dipping nodal plane that

Table 2. *P*-wave arrival time data used to locate the mainshock nucleation point. (a) Data believed *a priori* to be reliable. (b) Data believed *a priori* to be unreliable. Dm is epicentral distance from the ISC location for the mainshock, in degrees; Tm and Ta are the second part of *P*-wave arrival time for the mainshock and aftershock; Am is take-off azimuth away from the mainshock, in degrees; and Rm and Ra are residuals for the mainshock and aftershock, in seconds, reported by the ISC. Positive residuals mean observed arrival time was later than expected. Data categories 1–5 are defined in the text.

	Dm	Tm	Ta	Am	Tm-Ta	Rm	Ra	Notes
(a) Data believed a priori to be reliable								
DUI	1.03	14.5	0.3	321	14.2	1.8	1.4	1
ORI	1.18	14.5	4.5	133	10.0	-0.6	1.8	
AQU	2.07	30.6	17.0	317	13.6	2.0	2.2	1
RMP	2.19	30.5	16.2	296	14.3	0.2	-0.2	
MNS	2.50	35.5	21.5	308	14.0	0.7	0.6	1
MES	2.67	34.8	22.6	176	12.2	-2.3	-1.5	
OII	2.72	35.4	23.7	174	11.7	-2.5	-1.2	
GIB	3.05	42.2	29.0	200	13.2	-0.4	-0.3	
SDA	3.34	48.0	35.1	68	12.9	1.3	1.5	1
SDA	3.34	48.0	35.1	428	12.9	1.3	1.5	1
TIR	3.46	48.0	36.5	80	11.5	-0.5	1.0	
TIR	3.46	48.0	36.5	440	11.5	-0.5	1.0	
SRN	3.70	53.7	42.3	104	11.4	1.8	3.3	
PHP	3.94	54.7	42.6	76	12.1	-0.5	0.4	
PHP	3.94	54.7	42.6	436	12.1	-0.5	0.4	
KKS	4.01	55.4	43.4	71	12.0	-0.8	0.3	
KKS	4.01	55.4	43.4	431	12.0	-0.8	0.3	
OHR	4.15	57.5	46.5	85	11.0	-0.7	1.3	
OHR	4.15	57.5	46.5	445	11.0	-0.7	1.3	
KBN	4.18	59.6	48.4	91	11.2	1.0	2.8	
FIR	4.19	62.5	46.0	315	16.5	3.7	1.0	
PRT	4.35	63.5	48.5	315	15.0	2.4	1.3	
SKO	4.73	66.0	53.5	74	12.5	-0.4	0.1	
SKO	4.73	66.0	53.5	434	12.5	-0.4	0.1	
CEY	4.92	68.1	56.0	353	12.1	-1.0	0.6	
TRI	4.98	68.0	55.4	347	12.6	-2.0	-0.8	
LJU	5.21	72.1	59.3	354	12.8	-1.2	-0.2	
BEO	5.46	16.6	4.0	42	12.6	-0.2	0.5	
BEO	5.46	16.6	4.0	402	12.6	-0.2	0.5	
VAY	5.49	15.0	2.0	83	13.0	-2.2	-2.2	1
VAY	5.49	15.0	2.0	443	13.0	-2.2	-2.2	1
CTI	5.83	20.8	7.5	334	13.3	-1.2	-0.7	
PCN	5.90	25.0	10.0	317	15.0	2.1	1.0	
SAL	5.90	22.0	9.0	325	13.0	-0.9	-0.1	
SSR	6.18	25.0	13.0	48	12.0	-1.9	-0.7	
SSR	6.18	25.0	13.0	408	12.0	-1.9	-0.7	
OGA	6.76	33.6	21.0	334	12.6	-1.5	-0.3	
MOA	7.03	37.9	24.0	354	13.9	1.0	-1.1	
BHG	7.08	38.6	27.0	346	11.6	1.0	1.2	
SRO	7.27	43.4	27.0	16	16.4	1.1	-1.7	
SRO	7.27	43.4	27.0	376	16.4	1.1	-1.7	
GAP	7.29	41.9	31.8	337	10.1	-0.6	3.1	
KDZ	7.59	47.0	34.0	441	13.0	0.2	0.2	
KDZ	7.59	47.0	34.0	81	13.0	0.2	0.2	
DIM	7.80	49.0	36.0	78	13.0	0.6	-0.6	
DIM	7.80	49.0	36.0	438	13.0	0.6	-0.6	
FUR	7.85	49.8	35.7	340	14.1	-0.6	-0.9	
KHC	8.36	54.9	41.3	352	13.6	-2.6	-2.5	1
WET	8.46	55.3	41.7	349	13.6	-3.6	-3.4	1
MLR	9.03	65.8	55.0	56	10.8	-1.0	1.4	
MLR	9.03	65.8	55.0	416	10.8	-1.0	1.4	
PRU	9.14	65.2	51.5	357	13.7	-3.2	-3.1	1
BAF	9.17	66.4	54.0	322	12.4	-2.4	-0.9	
PRA	9.23	67.0	54.0	356	13.0	-2.6	-1.8	1
BUH	9.30	67.7	55.0	330	12.7	2.8	-1.6	
ECH	9.38	68.9	55.5	324	13.4	2.7	-2.2	3
KRA	9.75	16.7	4.4	18	12.3	0.1	1.3	
KRA	9.75	16.7	4.4	378	12.3	0.1	1.3	
KSP	10.01	18.5	6.5	4	12.0	-1.7	0.0	
KSP	10.01	18.5	6.5	364	12.0	-1.7	0.0	
BRG	10.06	17.9	5.0	355	12.9	-3.0	-2.2	1
MOX	10.12	19.3	8.0	346	11.3	-2.5	0.0	
CLL	10.57	24.9	11.0	352	13.9	-3.1	-3.2	1
DOU	11.90	46.4	33.3	324	13.1	0.3	1.1	
(b) Data believed a priori to be unreliable								
PRG	3.13	45.0	36.0	317	9.0	1.3	6.2	2
VLO	3.20	45.4	36.5	96	8.9	0.7	4.8	2
PRO	3.54	50.3	47.0	330	3.3	0.8	1.4	4
SOP	6.88	35.0	28.0	7	7.0	-1.7	4.9	2
SOP	6.88	35.0	28.0	367	7.0	-1.7	4.9	2
ORO	7.17	40.0	35.0	314	5.0	-0.9	8.0	2
VKA	7.44	43.3	26.0	5	17.3	-1.3	-4.9	5
VKA	7.44	43.3	26.0	365	17.3	-1.3	-4.9	5
CMP	8.36	60.0	36.0	55	24.0	2.5	-8.3	5
CMP	8.36	60.0	36.0	415	24.0	2.5	-8.3	5
MDB	8.43	60.0	50.0	48	10.0	1.5	4.8	4
MDB	8.43	60.0	50.0	408	10.0	1.5	4.8	4

was probably the fault plane (nodal planes were fitted with strike 310° dip 80° and strike 179° dip 15°). These four stations all plot on the focal sphere near this NE-dipping plane, and the resulting near-nodal ray path geometry probably caused low amplitudes and may thus explain the late arrival-time picks. In Category (3), at ECH, *P*-wave arrival time for the aftershock was reported almost 60 s too late. This obvious timing error can be corrected by subtracting one minute from the reported arrival time, to give the time shown in Table 2. Data from this station are therefore included. In category (4), at PRO and MDB, the aftershock arrival time is ~10 s late. This may either be a timing error from misreading a 10 s time marker (which could potentially be corrected by subtracting 10 s), or a late picking error. Because it is not possible to resolve the cause of these errors, these data are excluded. In Category (5), at CMP and VKA, *P*-wave arrival times for the aftershock are ~5–10 s early. This may be caused by misreading a 10 s time marker, in the case of VKA possibly in association with a late picking error for the aftershock. Because the cause of error in these data cannot be uniquely identified, they are also excluded. To include them while excluding the data in

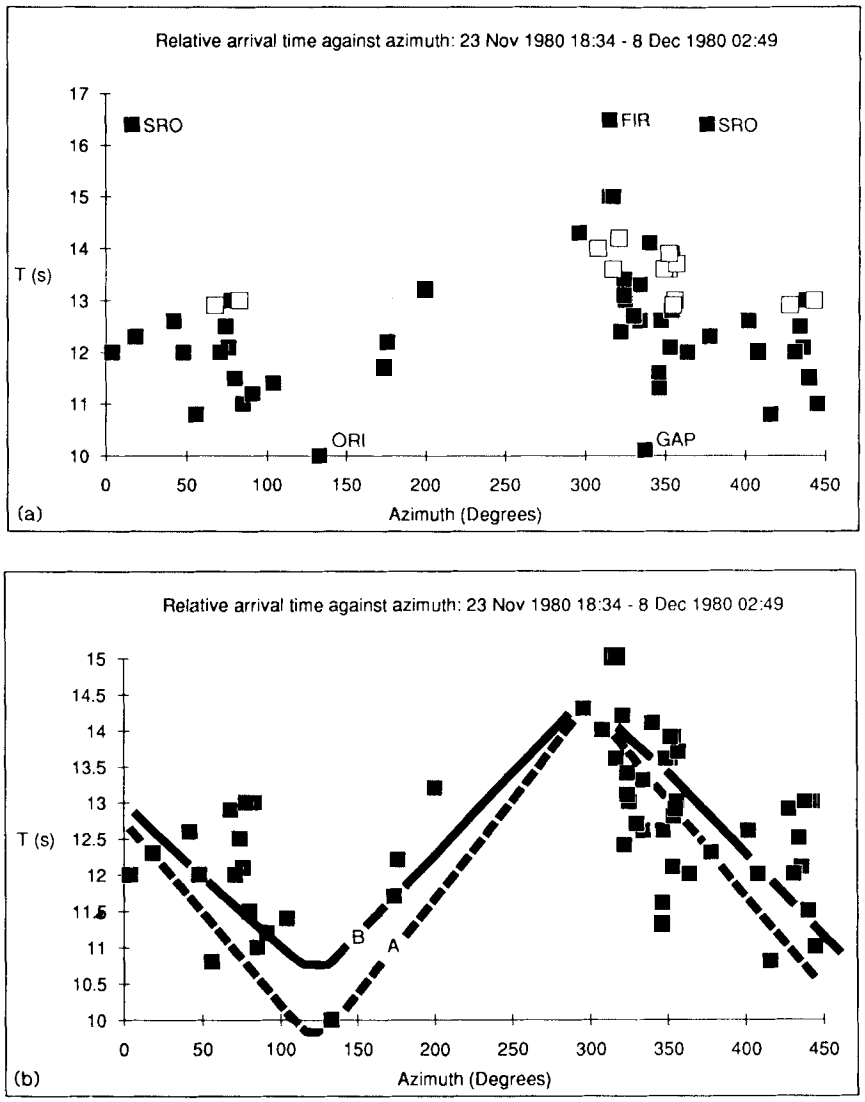

Figure 2. Plots of relative arrival time against azimuth for the mainshock and the December 8 aftershock, showing lateral variations that are primarily caused by the mainshock nucleation point being offset SE of the aftershock hypocentre, but which are also affected to some extent by timing and picking errors. (a) Including all data from the distance 1°–12° except the Category (2), (4) and (5) data in Table 2. Category (1) data, believed *a priori* to be probably the most reliable, are indicated using open symbols. (b) Excluding data from FIR, GAP and SRO, and including curves A and B fitted by eye through the remaining data. Note that some Category (1) data lie well away from the fitted curves, indicating that they are not necessarily the most reliable. Note that azimuths 0°–90° and 360°–450° are equivalent. Curve B matches better the data from this azimuth range (which is repeated), whereas curve A matches better the data from azimuth range ~300°–360° (which is only displayed once). Repetition of the fraction of the data that matches curves B better gives the misleading impression (which should be discounted) that overall the data matches curve B better than curve A. The azimuth range 0°–90° is repeated to facilitate comparison with adjacent azimuths. See text for discussion.

Category (4) would potentially bias the overall data distribution.

Figure 2(a) shows relative arrival time Δt against azimuth for all stations listed in Table 1 except those in Categories (2), (4) and (5), which were rejected for unreliability. The data distribution is fairly diffuse, including apparent outlying points from FIR, GAP, ORI and SRO. The low value of Δt at GAP is caused by the +3.1 s residual for the aftershock. Its *P*-wave arrival time is likely to have been picked late. The high value of Δt at FIR is caused by the +3.7 s residual for the mainshock. This is likely to be either a picking or a timing error. Although the cause of the outlier at SRO is difficult to judge, this point lies so far away from others for stations at similar azimuths that it can reasonably be regarded as erroneous. However, there is nothing about the point for ORI, either considering its residuals or its consistency with neighbouring points, that clearly establishes it as erroneous. Fig. 2(b) contains the same data as 2(a), except it omits the points for FIR, GAP and SRO that can reasonably be excluded: 46 data are plotted altogether, substantially fewer than the 63 used by us (1987). 11 of the excluded data are from the distance range 1°–12°, having been identified as unreliable in the above analysis. The other data, from more distant stations, are not considered

here: they correspond to the distance range 19°–39° where take-off angle varies strongly and ray paths are typically steeper, making relative arrival time less sensitive to separation of the two events.

It can be reasonably assumed *a priori* that the sine curve to be fitted to the data in Fig. 2(b) has phase ~210°, corresponding to the mainshock nucleation point being ~S60°E of the aftershock. Two important constraints restrict the range of curves that can be reasonably fitted by eye. First, the information available *a priori* suggests that the second part of relative origin time is ~12.0–12.5 s (Table 1). Any sine curve fitted should thus oscillate about a basline at Δt 12.0–12.5 s. Second, the trend of the numerous data from the NW quadrant requires the peak of the fitted sine curve to be at $\Delta t \sim 14.25$ s. However, because fewer data are available from stations to the south, the trough of the sine curve is less well defined. If this curve is fitted through the point from ORI (curve A), its trough is at $\Delta t \sim 9.75$ s. Its baseline is then at Δt 12.0 s and peak-to-peak amplitude is 4.5 s corresponding to 18 km separation. If a sine curve is fitted instead through the trend of the data from the NE quadrant, its trough is at $\Delta t \sim 10.75$ s. Its baseline is then at Δt 12.5 s and peak-to-peak amplitude is 3.5 s corresponding to 14 km separation. Without making a value judgement as to the relative reliability of station ORI (in southern Italy) against the stations in the NE quadrant (which are mostly in eastern Europe), analysis cannot proceed further.

One could fit the data numerically instead of by eye. One would then need to consider procedure in detail: should the curve to minimize least-square mismatch or absolute mismatch instead? Should one use a Gaussian weighting scheme to downweight data that are far from any fitted curve? If so, should all data be weighted in the same manner or should the Gaussian weighting reflect the perceived reliability of each station? How should constraints on relative origin time that exist *a priori* be built into the fitting procedure? Whatever scheme is used, the resulting fitted curve ought not to differ much from A or B in Fig. 2(b), because these curves are primarily consequential to well-defined constraints.

The standard error ellipse for our (1987) preferred nucleation point had typical radius ~2 km, and the estimated random error in both revised positions of the nucleation point is ~1 km. The 5–9 km offset of these revised locations SE of our (1987) preferred position thus exceeds the uncertainties in the individual locations, indicating that this offset is significant and warrants explanation. Apart from the difference in distance range of stations used, the principal difference in method concerned the procedure adopted for weighting each of the data in our (1987) location according to its perceived reliability (see Westaway 1985). With the exception of some obviously discrepant data that were excluded entirely, each *P*-wave arrival time used in our (1987) location was assigned a Gaussian weight factor W on the basis of the difference δt between the *P*-wave residuals for the ISC locations of the two events, where $W = \exp[-\delta t^2/(2\Delta T^2)]$ with ΔT chosen as 1.0 s. This choice of ΔT led to data with relative residuals $<\sim 1$ s being more or less fully weighted, whereas those with relative residuals $> \sim 3$ s contributed negligibly. This procedure avoided downweighting data from stations where residuals for both earthquakes were large but similar, which, as noted above, is not evidence for unreliability. However, it had the undesirable feature (which was not appreciated at the time) that large residuals that arose at some stations (e.g., MLR, ORI and SRN) because the ISC locations for individual events were mislocated would cause those stations to be downweighted. The data that were disregarded in Table 2 as obviously discrepant were also excluded from our (1987) location, with the exception of VKA that was included but where the value of δt would cause downweighting. Data from the three stations FIR, GAP and SRO [which were excluded from Fig. 2(b) for reasons that were not apparent from inspection of *P*-wave residuals] were included in our (1987) location but at reduced weight. Our (1987) location thus included some data that now appear bad and downweighted other data that now appear good.

One effect of our (1987) location downweighting data that now appear good would be to increase elements of the covariance matrix for this (1987) location, which depend inversely on the weighted partial derivatives of traveltime with respect to hypocentral coordinates. This may explain why the formal uncertainty in hypocentral coordinates for our (1987) location exceeds the uncertainty in the revised locations, even though these revised locations used fewer data. A second apparent effect of the Gaussian weighting used in our (1987) location was to reduce the amplitude of the best-fitting sine curve through the data relative to that in Fig. 2(b), causing lower separation of the two events. This probably occurred because stations to the south near the troughs of the sine curves in Fig. 2(b) (such as MLR, ORI, and SRN) had large relative ISC residuals and thus were downweighted by our (1987) procedure, whereas stations elsewhere with smaller relative residuals were not downweighted as much for this reason. The two principal differences between our (1987) location and the revised locations, the smaller separation of the two epicentres and the larger formal standard errors in our (1987) location, are thus explicable as artifacts of the weighting procedure used in our (1987) location.

3 IMPLICATIONS FOR THE SEQUENCE OF FAULT RUPTURES

We (1987) suggested that the early part of the teleseismic body wave records began with an initial subevent lasting 4 s, with M_o 2.5×10^{18} Nm, followed by a second subevent, which initiated 2.5 s later, was concentrated ~8 km NW of the first, and had M_o 6.2×10^{18} N m. A third subevent, which initiated 6.8 s after, and 14 km NW of, the first, had M_o 4.5×10^{18} N m and duration 4.6 s. In view of our (1987) preferred position of the fault rupture nucleation point, which was near a downdip projection of the Marzano fault, we (1987) suggested that the initial rupture occurred on the Marzano fault, and the second and third ruptures occurred on the Picentini fault. Nucleation point positions A and B are ~5–9 km SE of the our (1987) preferred location 4. They are near a downdip projection of the Carpineta scarp, where surface faulting was first repoted by Pantosti & Valensise (1990a): A is near a downdip projection of the SE end of this fault, and B is near a downdip projection of its NW end. Location A thus requires that mainshock rupture

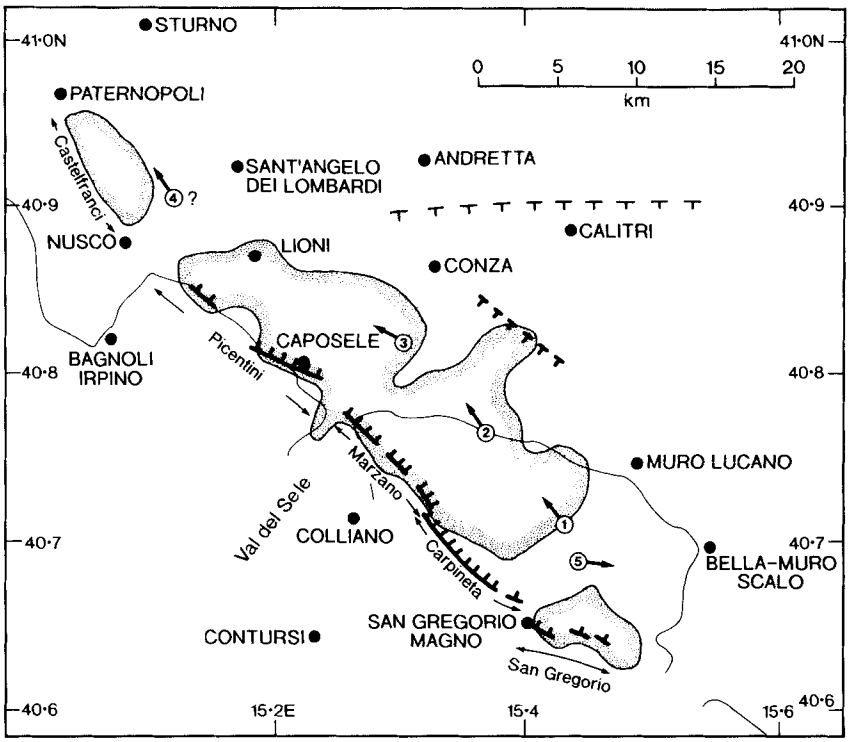

Figure 3. Summary map of the epicentral area indicating my preferred working hypothesis for the 1980 earthquake. Numbered arrows indicate suggested nucleation points and rupture directions for the four or five subevents that ruptured steep NE-dipping normal faults. Thick lines denote observed surface faulting, with hanging wall ticks, from Pantosti & Valensise (1990a). Dashed thick line with ticks indicates the position of the antithetic fault that Bernard & Zollo (1989) suggested ruptured in the 40 s subevent. Dashed thin line with ticks denotes an apparent SSW dipping normal fault at the north margin of the Cairano Pliocene sedimentary basin (see figs 25 and 26 of Westaway & Jackson 1987). This fault appears to have had no involvement in the 1980 earthquake. Shading enclosed by a thin line denotes the area of most intense aftershock activity, simplified from Westaway (1985) and Westaway & Jackson (1987). Its northwestern limit is outside the temporary seismograph network, and is thus poorly constrained. Although stations were deployed relatively sparsely to the southeast, the marked southeastern limit of aftershock activity lies well within the network, and is thus well defined. Thin line denotes the NE limit of the Campania–Lucania carbonate platform, also from Westaway & Jackson (1987). Note the alignment of the SE edge of the aftershock area with the surface faulting on the Marzano fault segment (first noticed by Westaway & Jackson 1984), and the similar alignment on the parts of the Picentini segment where surface faulting is exposed (unnoticed until now). See text for discussion.

nucleated on the Carpineta fault (Fig. 3), but location B is consistent with either the Marzano fault or the Carpineta fault having ruptured first.

For a fault rupture with known downdip length H and along-strike length L, with average slip u in rock with shear modulus μ, seismic moment M_o can be estimated as the product μuLH. Given the typical ~1 m of vertical slip observed in the field on the Marzano fault, and given its ~10 km length, ~10 km vertical extent, and likely shear modulus $\sim 3 \times 10^{10}$ Pa, we (1987) suggested that expected seismic moment released on it would be $\sim 3 \times 10^{18}$ N m, apparently confirming our (1987) waveform modelling. This reasoning and the relative positions of the second and third subevents, which released more seismic moment, led us (1987) to suggest that they both occurred on the Picentini fault. However, two principal factors invalidate this comparison. First, as already noted, work by Ward & Barrientos (1986) [which we (1987) did not consider] shows that slip at the earth's surface on a normal fault with ~60° dip embedded in an elastic half-space is roughly half the maximum slip on the fault at depth. Average slip on each fault that slipped in the 1980 earthquake is taken as ~1.7 times the slip at the earth's surface, to account for this factor in a manner that is approximately consistent with the results of Ward & Barrientos (1986). Second, but of less importance, with 60° fault dip, u equals the vertical slip divided by sin(60°) and H equals the brittle layer thickness divided by sin(60°). Allowing for both these effects adjusts the field estimate for seismic moment released on the Marzano segment to $\sim 6\text{–}7 \times 10^{18}$ N m, similar to the seismic moment released in the second subevent in our (1987) teleseismic waveform modelling. With vertical slip 0.5 m on the Carpineta fault (Pantosti & Valensise 1990a), this reasoning predicts $< \sim 3 \times 10^{18}$ N m seismic moment release there, similar to the seismic moment released in the first subevent of our (1987) teleseismic waveform modelling.

Comparison of the seismic moments observed in the first two subevents identified in our (1987) teleseismic waveform modelling with the values predicted from field evidence suggests that the first ruptured the Carpineta fault and the second ruptured the Marzano fault, regardless of whether location A or B is preferred. If location A is correct, the initial rupture nucleated near the SW end of the Carpineta fault and propagated northwest. Alternatively, if location B is accepted, rupture in the first subevent propagated southeastward along the Carpineta fault. It thus remains

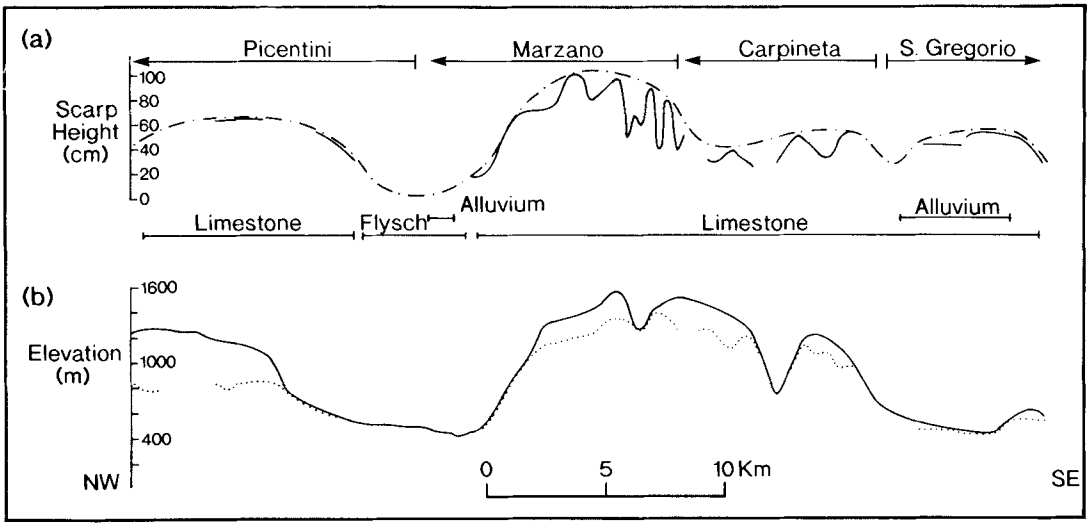

Figure 4. Profiles of scarp height (a) and topography (b) for the San Gregorio, Carpineta, Marzano, and Picentini scarps. In (a), the solid curve denotes scarp observations, and the dashed curve estimates original scarp height before degradation, providing a measure of u_z, the vertical slip at the earth's surface, at each locality. In (b), the dotted curve is scarp elevation above sea level, and the solid curve is elevation above sea level of the crest of the footwall escarpment near the scarp. The difference between these two curves gives an estimate of total throw across each fault. Note that although the Marzano and Picentini scarp heights in 1980 have ratio ~2:1, footwall escarpment heights are roughly equal. Redrawn from fig. 6 of Pantosti & Valensise (1990a).

unclear at this stage whether the Carpineta fault rupture propagated northwestward or southwestward. The relative position for the third subevent from our (1987) teleseismic waveform modelling, suggests that it should be associated with the Picentini scarp (Figs 3 and 4).

Table 3 compares field estimates for seismic moment released on the Carpineta, Marzano, and Picentini faults with seismic moments estimated by our (1987) teleseismic waveform modelling. Field estimates are calculated as $\mu L(H/\sin\delta)(cu_z/\sin\delta)$, where μ is the assumed shear modulus (3×10^{10} Pa), L and H are the along-strike length and vertical extent of the fault, u_z is the vertical slip, δ is the dip of the fault, and the factor c of ~1.7 approximately converts slip at the earth's surface to average slip. The two sets of seismic moment estimate match well. The separation of the mid points of the Carpineta and Marzano faults observed in the field (9 km) also approximates the offset in the NW direction between the first two subevents in our (1987) teleseismic waveform modelling (8 km).

Table 3. Seismic moment release on individual normal faults.

Number+Name	L (km)	u_z (m)	$M_0(F)$ (10^{18} Nm)	$M_0(S)$ (10^{18} Nm)	ϕ (°)	ψ	t (s)	M_w
1. Ruptures on faults dipping northeast at ~60°								
1. Carpineta	9	0.5	2.4	2.5	315	NW	0	6.2
2. Marzano	10	1.0	6.7	6.2	315	NW	2.5	6.5
3. Picentini	14	0.6	4.5	4.5	300	NW	6.8	6.4
(4. Castelfranci	~8	~0.5	~2.2	~2.0	330	NW	~12.8?	6.2)
5. San Gregorio	7	0.5	1.9	(2.0)	300	SE	~0?	6.2
TOTAL	40-48		15.5-17.7	15.2-17.2				
2. Rupture dipping northeast at 20° at base of brittle layer								
20 s subevent				4.0	315	NE	~19	6.4
3. Rupture on fault dipping southwest at ~70°								
40 s subevent				3.0	135	?	~38	6.3
TOTAL				22.2-24.2				

L is along-strike length; u_z is vertical slip, observed or estimated, at the earth's surface; $M_0(F)$ and $M_0(S)$ are field and seismological estimates for seismic moment; ϕ is strike; ψ is rupture direction; t is nucleation time after the initial rupture initiated; and M_w is moment–magnitude calculated from M_0 using Hanks & Kanamori's (1979) equation. If the Carpineta and Marzano ruptures are counted together, they have M_w 6.6.

Fault ruptures in the brittle upper crust typically propagate at ~3 km s^{-1}. Rupture of the ~8 km distance northwestward along the Carpineta segment from nucleation point 1 in Fig. 3, which is consistent with location A, would be expected to take ~2.7 s, which is similar to the 2.5 s interval between the first and second subevents in our (1987) teleseismic waveform modelling. If location A is preferred, this suggests that rupture propagated continuously northwestward from the Carpineta fault to the Marzano fault. In contrast, if location B were adopted instead, the similarity of the delay between the first two subevents observed teleseismically and the time required to rupture the Carpineta fault must be regarded as a coincidence. Although not conclusive, my preference is thus that the initial rupture nucleated at the SE end of the Carpineta fault (location A), because as well as matching the field and seismological estimates for seismic moment this choice can also explain the delay between the first and second subevents that are observed teleseismically.

The following preferred description of the first three subevents of the earthquake is consistent with location A for the fault rupture nucleation point, the field evidence of faulting, and the teleseismic waveform modelling. Fault rupture initiated at or near the SE end of the Carpineta fault and propagated NW, releasing ~2.5×10^{18} N m seismic moment with ~0.5 m of vertical slip at the earth's surface and taking ~2.5 s to reach the NW end of this fault. Rupture then propagated without interruption onto the Marzano segment, releasing ~6.5×10^{18} N m of seismic

moment with ~1 m of vertical slip at the earth's surface. Rupture would have thereby taken ~6.3 s to cover the total 19 km length to the NW end of the Marzano fault. At this point the rupture paused for ~0.5 s, before a second rupture initiated on the Picentini fault, causing ~0.6 m vertical slip and releasing $\sim 4.5 \times 10^{18}$ N m seismic moment, probably dying out where the uniform NW trend of the Picentini range front is interrupted by a southwestward step near Nusco (see Fig. 3 and plate 1 of Westaway & Jackson 1987).

The timing of slip on the San Gregorio fault remains problematical. We (1987) suggested, on the basis of teleseismic waveform modelling and analysis of timing of accelerograms, that this rupture initiated 12.8 s after the first subevent nucleated. However, as already noted, Bernard & Zollo (1989) disputed our (1987) accelerogram timing scheme. The field estimate for seismic moment on the San Gregorio fault, only $\sim 2 \times 10^{18}$ N m, is so small that, provided this fault rupture occurred within ~15 s of the first subevent, it can be concealed more or less anywhere within synthetic body wave seismograms, being overwhelmed by the larger Marzano and Picentini fault ruptures. It seems plausible that the San Gregorio rupture initiated shortly after rupture on the nearby Carpineta fault, and was probably masked in the teleseismic records by signal from one of the larger fault ruptures.

Bernard & Zollo's (1989) suggested relative timing scheme for the 20 s subevent and the first subevent placed it ~20 km SE of the nucleation point for the first subevent. They (1989) consequently placed the 20 s subevent 20 km SE of our (1987) preferred nucleation point for the first subevent, in a position consistent with the San Gregorio fault. However, with the revised nucleation point for the first rupture 5–9 km SE of our (1987) nucleation point, Bernard & Zollo's (1989) timing scheme requires the 20 s subevent to be shifted ~5–9 km farther SE also, making it ~2–6 km SE of the southeastern end of the San Gregorio fault scarp, beyond the concentrated aftershock activity. Neither we (1984, 1987), nor Pantosti & Valensise (1990a) found any evidence for faulting SE of the San Gregorio scarp. One may choose to believe that the timing scheme proposed by Bernard & Zollo (1989) is correct, provided one is prepared to accept that the 20 s subevent involved fault rupture only at depth, which was not associated with aftershocks. Alternatively, one may judge their timing scheme to be mistaken, in which case no evidence exists that links the 20 s subevent, identified seismologically, with faulting at San Gregorio or at any other point farther southeast. Given that other timing schemes have been suggested that differ from that by Bernard & Zollo (1989), my preference is for the second of these alternatives.

We (1987) suggested, on the basis of the timing of ground acceleration, that the 40 s subevent nucleated ~8–16 km from the first subevent, at some azimuth between north and N40°E. We adopted the nominal position ~12 km north of the nucleation point of the first subevent for our (1987) waveform modelling. Bernard & Zollo (1989) estimated the separation of the first and 40 s subevents as ~8 km toward N10°E, which lies within the broader region suggested by us (1987). Bernard & Zollo (1989) also noted seismological observations, and observations of elevation change and geomorphology, which they suggest require that the 40 s subevent involved slip on a steep SW-dipping normal fault

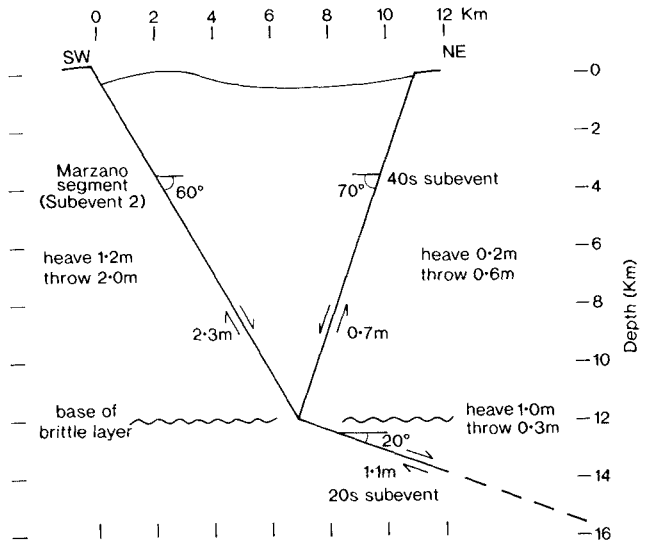

Figure 5. Schematic cross-section across the Marzano fault and its associated antithetic fault ~11 km farther NW, which appears to have ruptured in the 40 s subevent of the 1980 earthquake. Heave, throw and slip are estimates at depth and exceed those at the surface. See text for discussion.

that passed a few km south of Calitri (Fig. 3). These pieces of evidence appear reasonable. However, as with the 20 s subevent, if their (1989) position for the 40 s subevent is shifted ~5–9 km southeast to take account of the revised nucleation point of the first subevent, it ceases to match the other observations that support their suggested location for the 40 s subevent. This suggests that their analysis of acceleration timing for the 40 s subevent is mistaken, also. However, the other, reliable, observations indicate that the 40 s subevent occurred on a steep normal fault with SW dip, which is situated opposite the Marzano fault, the two faults being ~11 km apart at the earth's surface but adjoin at the base of the brittle layer (Fig. 5).

In the absence of convincing evidence to the contrary it seems reasonable to return to our (1987) suggestion that the 20 s subevent occurred on a low-angle surface at the base of the brittle layer, situated NE of the Marzano fault. This position is directly beneath the steep SW-dipping fault that ruptured in the 40 s subevent (Fig. 5). The consequences of this suggestion are discussed in Section 4.

4 DISCUSSION

Along-strike extent of faulting

Opinions have differed strongly as to the likely along-strike extent of coseismic faulting in the 1980 mainshock. Pantosti & Valensise (1990a) reported that there was no evidence of surface faulting either NW of the NW end of the Picentini range front or SE of the SE end of the San Gregorio scarp, making the along-strike length of faulting ~40 km. In contrast, others who have modelled accelerograms of the 1980 mainshock have proposed much longer extents of faulting. For example, Suhadolc, Vaccari & Panza (1988), Panza & Suhadolc (1989), Vaccari, Suhadolc & Panza

(1990) and Harabaglia *et al.* (1990) have all suggested ~70 km total length.

The accelerograms from Sturno (Fig. 3) are potentially of crucial importance for the understanding of this earthquake. Observed peak horizontal ground acceleration (PHGA) at this station exceeded 3 m s^{-2} (Westaway & Smith 1989). Sturno is ~15 km from the closest point on a surface projection of the Picentini fault, and ~28 km from the closest point on a surface projection of the Marzano fault. If the Marzano rupture had occurred in isolation, it seismic moment and equivalent magnitude (Table 3) would be expected to cause barely ~1 m s^{-2} of PHGA at this distance. Similar PHGA would also be expected if the Picentini fault rupture had occured in isolation (using Joyner & Boore's 1981 equation: see Westaway & Smith 1989). Given this discrepancy, we (1987) suggested that the high PHGA at Sturno may have been a directivity effect of the rupture on one or both of these faults propagating toward Sturno. Subsequent modelling of ground acceleration records (e.g., Siro & Chiaruttini 1989; Vaccari *et al.* 1990; Harabaglia *et al.* 1990) appears to indicate, in contrast, that PHGA at Sturno was caused by a relatively small fault rupture nearby. The Castelfranci fault (Fig. 3), which is identified on the basis of its aftershock cluster, seems a strong candidate for this nearby fault rupture, with the closest point on its surface projection ~6 km from Sturno. Given its likely $M_o \sim 2 \times 10^{18}$ N m (estimated in Table 2 assuming 0.5 m vertical slip, 60° fault dip, and 8 km along-strike extent) that is equivalent to $M_w \sim 6.2$ (using Hanks & Kanamori's 1979 equation), ~3 m s^{-2} PHGA is predicted (using Joyner & Boore's 1981 equation), as is observed at Sturno.

Our (1987) teleseismic waveform modelling suggested a fourth fault rupture subevent with seismic moment 2×10^{18} N m initiated 12.8 s after the initial subevent. We (1987) suggested that this occurred on the San Gregorio fault. However, our 6.8 s initiation time and 4.6 s duration for the Picentini rupture suggest that this rupture died out at the NW end of the Picentini fault ~ 11.4 s after the first rupture initiated. If this poorly resolved 12.8 s subevent is associated instead with the Castelfranci fault, then its timing suggests a ~1.4 s delay at the NW end of the Picentini fault, before rupture propagation resumed.

Most ground acceleration modelling that has been carried out to date treats virtually every aspect of the earthquake as a free parameter, including some (such as fault dip and strike) that are in fact tightly constrained. Hopefully, such modelling in future will instead use results for the overall fault rupture geometry that are based on independent evidence (such as that shown in Fig. 3) to provide key constraints, and will concentrate on resolving aspects of the earthquake where substantial genuine uncertainties remain (primarily, the detailed rupture timing).

In this context, it should be noted that the NW limit of the Castelfranci aftershock cluster is poorly resolved: at this extreme NW position aftershocks are beyond most of the temporary seismograph network and are thus poorly located (Westaway 1985), and any real clustering there may have been smeared out by mislocation. The true NW limit of the Castelfranci fault may thus be a few kilometres NW of the position shown in Fig. 3. However, it appears most unlikely that the total length of faulting was ~70 km.

Extent of 'missing' seismic moment

Some people (e.g. Pantosti & Valensise 1990a) have noted apparent discrepancies between the total scalar seismic moment of the earthquake, which is $\sim 26 \times 10^{18}$ N m (Westaway & Jackson 1987) and the sum of field and seismological estimates for seismic moment of individual fault ruptures (Table 3). The sum of seismic moments for the three relatively well-documented subevents (Carpineta, Marzano and Picentini) is ~ 13.2–13.6×10^{18} N m. Allowing $\sim 2 \times 10^{18}$ N m for each of the apparent fault ruptures at San Gregorio and Castelfranci, total scalar seismic moment released on NE-dipping normal faults was probably $\sim 17.6 \times 10^{18}$ N m. With 7×10^{18} N m additional seismic moment released in the 20 and 40 s subevents, total scalar seismic moment rises to $\sim 24.6 \times 10^{18}$ N m, within 5 per cent of the expected amount. Seismic moment estimates deduced by teleseismic waveform modelling are inherently uncertain by ~20 per cent (e.g. Westaway & Jackson 1987). Furthermore, the uncertainty as to whether a 10 or 12 km deep base of the brittle layer should be used to calculate field estimates of seismic moment, causes ~20 per cent uncertainty in these estimates. The 5 per cent discrepancy between the overall scalar seismic moment and the estimates based on individual subevents is thus not significant, and there are thus no grounds for suggesting that any additional fault rupture occurred elsewhere. Given these ~20 per cent margins of uncertainty, there is no need for slip on the Castelfranci fault to match the expected seismic moment. The aftershock cluster there, the results from the ground acceleration modelling, and the tentative reinterpretation of our (1987) teleseismic waveform modelling, support the existence of such a fault rupture. However, given the relatively short length of the Castelfranci fault, and the small amount of likely slip on it, the small seismic moment release expected may instead be masked by other larger ruptures, as seems likely for the San Gregorio rupture. I am carrying out more detailed waveform modelling to see whether positive teleseismic evidence exists for the San Gregorio and Castelfranci ruptures, and if possible to constrain their timing relative to the others. These results will be presented elsewhere.

Fault geometry at depth and coseismic extension rate

The Campania–Basilicata mainshock caused substantial along-strike variations in throw (Fig. 4) and heave, where throw and heave are, respectively, the vertical and horizontal components of slip. Given the ~60° dip of all documented surface faulting, throw and heave have the ratio cos(60°):sin(60°) or $\sqrt{3}$:1. The heave at the earth's surface at any locality is thus $1/\sqrt{3}$ times the throw. Heave and throw will maintain the same proportion at depth and, following the results of Ward & Barrientos (1986), typical heave at depth, like typical throw, will be roughly double that at the earth's surface. Heave was thus ~0.2 m at the earth's surface on the San Gregorio, Carpineta, and Picentini faults (suggesting ~0.4 m at depth). In contrast, heave at depth on the Marzano fault appears to have been ~1.2 m, to which ~0.2 m heave on the antithetic fault NE of the Marzano fault that apparently ruptured in the 40 s subevent, should be added, making ~1.4 m altogether (Fig.

5). Assuming the low-angle surface that ruptured in the 20 s subevent was approximately equidimensional, its seismic moment suggests ~1.1 m average slip, which gives ~1.0 m average heave. As already noted, Pantosti & Valensise (1990b) have shown that earthquakes similar to the 1980 event recur every ~1700 yr. With this interval and 1 m vertical slip at the earth's surface per earthquake, the age of the Marzano fault can be estimated as ~0.7 Myr (400 m vertical offset × 1700 yr interval / 1 m vertical slip per earthquake).

The brittle layer in the vicinity of the Marzano fault system thus apparently takes up ~1.4 m extension every ~1700 yr, making local extension rate in the brittle layer across this normal fault system ~0.8 mm yr^{-1}. However, with the fault geometry in Fig. 5 the lower crust beneath this 11 km wide fault system apparently extends by only ~0.4 m every ~1700 yr, giving extension rate ~0.2 mm yr^{-1} and extensional strain rate ~0.2 mm yr^{-1}/11 km or ~0.6×10^{-15} s^{-1}. The mismatch between estimated local extension rates in the brittle layer and in the lower crust requires extension in the lower crust to be taken up across a zone that is wider than this overlying fault zone in the brittle layer. Whether major historical earthquakes known to have affected the Campania–Basilicata region but which did not rupture the Marzano or San Gregorio faults, for example those in AD 990 and 1694 (Postpischl 1985), ruptured other faults that slipped in 1980 or different active normal fault segments *en echelon* to them, is unclear. The suggested 0.8 mm yr^{-1} extension rate of the brittle layer across the Marzano fault is thus a lower limit for extension rate across the southern Apennines, since the existence of other active normal fault segments *en echelon* to Marzano would indicate a higher overall extension rate.

Normal fault morphology

Some people (e.g. Ambraseys & Tchalenko 1972) have suggested that sense of stepping along fault scarps correlates with sense of the strike–slip component of slip: a left-lateral component is associated with rightward stepping. The Carpineta and Marzano scarps strike at ~315° and typically show stepping to the right every few hundred metres or more (Westaway & Jackson 1984, 1987; Pantosti & Valensise 1990a). We (1984, 1987) described one locality on the Marzano fault where striations on an exposed limestone surface indicate a small component of left-lateral slip. Such a component is supported by our (1987) first-motion focal mechanism, which had slip vector azimuth N37°E (Westaway, Gawthorpe & Tozzi 1989), and by our (1987) teleseismic waveform modelling.

Despite substantial variations in fault strike, slip vector azimuth remained roughly constant during the 1984 Lazio–Abruzzo earthquake sequence in central Italy (Westaway *et al.* 1989). It seems reasonable to assume that it remained constant in the Campania–Basilicata sequence of ruptures also. The San Gregorio scarp has typical strike ~300°, and, assuming the same slip vector azimuth, a component of right-lateral slip is expected instead. Strands of the discontinuous Picentini scarp have typical strike ~300° also, and a component of right-lateral slip is thus also expected there. The suggested Castelfranci fault farther NW has strike ~320°–330° instead, which would predict a greater proportion of left-lateral slip that was observed on the Marzano scarp. On both the Carpineta–Marzano and San Gregorio scarps, observed stepping sense is thus as expected given the observed or expected sense of the strike–slip component.

Normal fault segmentation

On a larger scale, it is worthwhile to try to subdivide the 1980 faulting into segments. Segmentation models have been proposed for normal faults elsewhere using evidence for independent rupturing patterns in earthquakes, geomorphology, and other criteria (e.g. Schwartz & Coppersmith 1984). However, use of different criteria by different authors sometimes leads to the deduction of different segmentation patterns for the same fault (see, e.g., DePolo *et al.* 1991). For example, Westaway & Jackson (1987) suggested that the San Gregorio and Marzano scarps should each be regarded as a fault segment, and the Picentini range front should count as a third fault segment (we did not then consider the potential significance of the aftershock cluster NW of Nusco, and were unaware of the Carpineta scarp). Pantosti & Valensise (1990a) suggested instead that the whole > ~40 km length of faulting in 1980 is a single segment. The criterion for establishing segmentation that will be used here is that of independent rupturing in major earthquakes, which may be demonstrable or deduced. Segment boundaries on other active normal faults elsewhere typically lie at discontinuities in strike or at points where faults step substantially (> ~1 km) *en echelon*, frequently exhibiting overlap between steps.

Using these criteria, the boundary between the Carpineta and San Gregorio faults, which shows a ~1 km rightward step and a ~20° change in strike, appears at first sight to be a strong candidate for a segment boundary. The boundary beneath the northern Sele valley, between the Marzano and Picentini faults, where the 1980 faulting also steps ~1 km rightward with a ~20° strike change, can also readily be regarded as a segment boundary. Although these two segments both ruptured in 1980, evidence from the timing of subevents identified by teleseismic waveform modelling suggests that rupture experienced a ~0.5 s delay at this boundary, rather than propagating continuously. Outcrop in the uplifted footwalls of both the Marzano and Picentini faults comprises Mesozoic crystalline limestone (e.g., Pantosti & Valensise 1990a), which resists erosion. The offset in topography across both faults (Fig. 4) will thus provide a reliable estimate of throw, which is at least as large on the Picentini fault as on the Marzano fault. However, only half as much slip occurred in 1980 on the Picentini fault as on the Marzano fault. Assuming a proportion of the earthquakes on these faults repeats the 1980 rupture pattern, the observed throws require other earthquakes to rupture the Picentini fault only. The Marzano and Picentini faults thus appear able to sometimes rupture independently, and can thus be deduced to be separate fault segments. The boundary between the Picentini and Castelfranci faults appears associated with a ~20° change in strike and a > 1 km sideways step also, and may have also been associated with a delay in the 1980 fault rupture. By analogy, it can also tentatively be regarded as a segment boundary.

The boundary between the Carpineta and Marzano scarps is more problematical. It is associated with a ~400 m rightward step, and the Marzano fault took up roughly twice as much slip as the Carpineta fault in 1980. Slip on the Marzano fault system also appears associated with low-angle and antithetic slip, whereas Carpineta appears to be a simple NE-dipping fault. However, if my preferred nucleation point for the initial fault rupture at the SE end of the Carpineta fault is accepted, the teleseismic waveform modelling indicates that rupture propagated continuously from the Carpineta fault onto the Marzano fault. In addition, the observation by Pantosti & Valensise (1990b) that the San Gregorio and Marzano faults have the same recurrence history appears to require the intervening Carpineta fault to share this recurrence history also. If the primary criterion for a segmentation model is to separate portions of fault that demonstrably rupture independently, the Carpineta and Marzano faults should be regarded as parts of the same fault segment, despite their different geometries and amounts of coseismic slip in 1980.

Categorization of the boundary between the Carpineta and San Gregorio faults is also problematical. As already mentioned, the local abrupt change in strike and the position of the initial rupture nucleation point near this boundary would normally be regarded as strong criteria for a segment boundary. However, the trenching by Pantosti & Valensise (1990b) establishes the same earthquake recurrence history on the San Gregorio fault as on the Marzano fault. Assuming that rupture in every such earthquake nucleated at the SE end of the Carpineta fault, this suggests that every time a NW-propagating rupture occurs on the Carpineta–Marzano fault, a smaller SE-propagating rupture is required on the San Gregorio fault. Despite the geomorphological evidence, using the criterion for segmentation of a demonstrably independent fault rupture history, the junction of the San Gregorio and Carpineta–Marzano faults appears not to be a segment boundary. Using this criterion, the 1980 earthquake can thus be regarded as having involved rupture of at least two NE-dipping normal fault segments: San Gregorio–Carpineta–Marzano, and Picentini.

This discussion highlights the need for consistent definition of terminology for fault segmentation (see also DePolo *et al.* 1991). A term is required for fault discontinuities like that at the junction of the San Gregorio and Carpineta faults, which is a nucleation point for major earthquakes and a marked discontinuity in faulting associated with a strike change and an *en echelon* step, but at which faults on either side do *not* rupture independently. A second term is required for fault discontinuities like that between the Marzano and Carpineta faults, where coseismic fault slip and overall fault geometry change abruptly, but where there is no change in fault strike and no evidence for independent rupturing in earthquakes. I suggest terminology in which a 'traditional' segment boundary, as defined e.g. by Schwarz & Coppersmith (1984), in terms of a demonstrably independent history of fault rupturing, should perhaps be reclassified as a category I fault discontinuity. A boundary such as that at the NW end of the San Gregorio fault, which despite the geomorphological evidence and the earthquake nucleation point location does not separate faults with independent rupture history, should be regarded as a category II fault discontinuity. A boundary such as that at the NW end of the Carpineta fault, which separates faults with the same strike but different overall geometry and different coseismic slip in individual earthquakes, should be regarded as a category III fault discontinuity. These suggestions of category II and III discontinuities, where changes in coseismic slip and in strike, and *en echelon* stepping, are observed, but which do not rupture independently, complicate the already difficult problem of establishing fault segmentation models on the basis of trenching or geomorphological evidence.

5 CONCLUSIONS

Re-examination of the *P*-wave arrival time data available to locate the nucleation point of the initial fault rupture in the 1980 Campania–Basilicata earthquake, using a revised relative location method, indicates that it was ~5–9 km SE of our (1987) preferred position, and was probably located near the SE end of the Carpineta fault scarp. Fault rupture subevents 1, 2 and 3 that were resolved in our (1987) teleseismic waveform modelling correspond to northwestward rupture on the Carpineta, Marzano and Picentini faults, which strike NW and dip NE at ~60°, with typical vertical slip and seismic moment on each fault estimated in Table 3. Rupture propagation appears to have experienced no delay at the NW end of the Carpineta fault, but experienced a ~0.5 s delay at the structural discontinuity at the NW end of the Marzano fault before resuming on the Picentini fault segment. This Picentini rupture probably died out at another structural discontinuity near Nusco, ~33 km from the initial nucleation point. Aftershock and ground acceleration evidence suggest a fourth NW-propagating fault rupture subevent at Castelfranci, beyond the NW end of the Picentini fault, which may have begun ~12.8 s after the initial rupture nucleated and thus ~1.4 s after rupture reached the NW end of the Picentini fault. The San Gregorio surface faulting was probably generated by a fifth fault rupture with similar orientation to the first three, which may have involved SE propagation and may have initiated around the same time as the Carpineta rupture. Two later subevents, ~20 s and ~40 s after the initial subevent nucleated, were associated with sources with different orientation. A previous suggestion that the 20 s subevent occurred on the San Gregorio fault is inconsistent with the revised nucleation point of the first subevent. The 20 s and 40 s subevents appear instead to have both occurred NE of the Marzano fault: the 20 s one apparently involved a low-angle rupture at the base of the brittle upper crust, whereas the 40 s one appears to have involved slip on a steep SW-dipping normal fault, the geometrical relationship of these faults being as shown in Figs 3, 4 and 5. Taken together, these six or seven subevents account for the overall scalar seismic moment of the earthquake.

ACKNOWLEDGMENTS

Some of the ideas presented in this article were developed following stimulating discussions with other participants at the 1990 November 'Irpinia Dieci Anno Dopo' tenth anniversary conference in Sorrento. I am particularly

grateful to Pascal Bernard, Daniela Pantosti, Dave Schwartz, Gianluca Valensise, and Aldo Zollo.

REFERENCES

Ambraseys, N. N. & Tchalenko, J. S., 1972. Seismotectonic aspects of the Gediz, Turkey, earthquake of March 1970, *Geophys. J.R. astr. Soc.*, **30,** 229–252.

Arca, S., Bonasia, V., Gaulon, R., Pingue, F., Ruegg, J. C. & Scarpa, R., 1983. Ground movements and faulting mechanism associated to the November 23, 1980 southern Italy earthquake, *Boll. Geod. Sci. Affini,* **42,** 137–147.

Bernard, P. & Zollo, A., 1989. The Irpinia (Italy) 1980 earthquake: detailed analysis of a complex normal faulting, *J. geophys. Res.*, **94,** 1631–1647.

DePolo, C. M., Clark, D. G., Slemmons, D. B. & Ramelli, A. R., 1991. Historical surface faulting in the Basin and Range province, western North America: implications for fault segmentation, *J. Struct. Geol.*, **13,** 123–136.

Eyidoğan, H. & Jackson, J. A., 1985. A seismological study of normal faulting in the Demirci, Alasehir and Gediz earthquakes of 1969–70 in western Turkey: implications for the nature and geometry of deformation in the continental crust, *Geophys. J.R. astr. Soc.*, **81,** 569–607.

Hanks, T. C. & Kanamori, H., 1979. A moment–magnitude scale, *J. geophys. Res.*, **84,** 2348–2350.

Harabaglia, P., Suhadolc, P. & Panza, G. F., 1990. Rupture process dynamics from inversion of accelerometric data. In *Proc. 'Irpinia dieci anno dopo' meeting,* Sorrento, Italy, 19–24 November 1990, pp. 73–78, Istituto Nazionale di Geofisica, Rome.

Herrin, E., 1968. Seismological tables for P phases, *Bull. seism. Soc. Am.*, **58,** 1193–1241.

Joyner, W. B. & Boore, D. M. 1981. Peak horizontal acceleration and velocity from strong-motion records including records from the 1979 Imperial Valley, California, earthquake, *Bull. seism. Soc. Am.*, **71,** 2011–2038.

Pantosti, D. & Valensise, G., 1990a. Faulting mechanism and complexity of the November 23, 1980, Campania–Lucania earthquake, *J. geophys. Res.*, **95,** 15 319–15 342.

Pantosti, D. & Valensise, G., 1990b. Source geometry and long term behavior of the 1980 fault based on field geologic observations, in *Proc. 'Irpinia dieci anno dopo' meeting,* Sorrento, Italy, 19–24 November 1990, pp. 45–50, Istituto Nazionale di Geofisica, Rome.

Panza, G. F. & Suhadolc, P., 1989. Realistic simulation and prediction of strong ground motion, in *Computers and Experiments in Stress Analysis,* pp. 77–98, eds Carlomagno, G. M. & Brebbia, C. A., Springer-Verlag, Berlin.

Postpischl, D., 1985. *Atlas of Isoseismal Maps of Italian Earthquakes,* Consiglio Nazionale Richiercha, Rome.

Schwartz, D. P. & Coppersmith, K. J., 1984. Fault behavior and characteristic earthquakes: examples from the Wasatch and San Andreas fault zones, *J. geophys. Res.*, **89,** 5681–5698.

Siro, L. & Chiaruttini, C., 1989. Source complexity of the 1980 southern Italian earthquake from the analysis of strong-motion S-wave polarization, *Bull. seism. Soc. Am.*, **79,** 1810–1832.

Suhadolc, P., Vaccari, F. & Panza, G. F., 1988. Strong motion modelling of the rupturing process of the November 23, 1980, Irpinia earthquake, in *Seismic Hazard in Mediterranean Regions,* pp. 105–128, ed. Bonnin, J., European Community, Brussels.

Vaccari, F., Suhadolc, P. & Panza, G. F., 1990. Irpinia, Italy, 1980 earthquake: waveform modelling of strong motion data, *Geophys. J. Int.*, **101,** 631–647.

Ward, S. N. & Barrientos, S. E., 1986. Inversion for slip distribution and fault shape from geodetic observations of the 1983 Borah Peak, Idaho, earthquake, *J. geophys. Res.*, **91,** 4909–4919.

Westaway, R., 1985. Active tectonics of Campania, southern Italy, *PhD thesis,* University of Cambridge, UK.

Westaway, R., 1987a. The Campania, southern Italy, earthquakes of 1962 August 21, *Geophys. J.R. astr. Soc.*, **90,** 375–443.

Westaway, R., 1987b. Comment on 'The southern Italy earthquake of 23 November 1980: an unusual pattern of faulting' by R. S. Crosson, M. Martini, R. Scarpa, and S. C. Key, *Bull. seism. Soc. Am.*, **77,** 1071–1074.

Westaway, R. & Jackson, J. A., 1984. Surface faulting in the southern Italian Campania–Basilicata earthquake of 23 November 1980, *Nature,* **312,** 436–438.

Westaway, R. & Jackson, J. A., 1987. The earthquake of 1980 November 23 in Campania–Basilicata (southern Italy), *Geophys. J. R. astr. Soc.*, **90,** 375–443.

Westaway, R. & Smith, R. B., 1989. Strong ground motion in normal faulting earthquakes, *Geophys. J.*, **96,** 529–559.

Westaway, R., Gawthorpe, R. & Tozzi, M., 1989. Seismological and field observations of the 1984 Lazio–Abruzzo earthquakes: implications for the active tectonics of Italy, *Geophys. J.*, **98,** 489–514.